Reanalysis of high-resolution XMM-Newton data of V2491 Cygni using models of collisionally ionized hot absorbers

Çiğdem Gamsızkan & Şölen Balman
Middle East Technical University, Dept. of Physics, Ankara, Turkey
cigdem.gamsizkan@gmail.com
solen@astroa.physics.metu.edu.tr

Abstract

The classical nova V2491 Cyg was observed twice by *XMM-Newton* RGS (Reflection Grating Spectrometer) on May 20.6 and May 30.3, 2008 in outburst. Our aim is to reanalyse the archival RGS data of this classical nova and model the complex absorption features that are seen in the high resolution X-ray spectra. The RGS data can be best fitted with two collisionally ionized hot absorber and a photoionized warm absorber model (plus a model for interstellar absorption and dust absorption) together with a blackbody model for the continuum. The two collisionally ionized hot absorption components have temperatures $kT_1 \simeq 1.0-3.6$ keV and $kT_2 \simeq 0.4-0.87$ keV with rms velocities $\sigma_{v1} \sim 872$ km s^{-1} and $\sigma_{v2} \sim 56$ km s^{-1}. We find blackbody temperatures in a range 61-91 eV yielding a white dwarf (WD) mass of 1.15-1.3 $M_\odot$, but our analysis on the second observation reveals a second blackbody component with effective temperature 120-131 eV and effective radius about 10% of the WD. The further details of the analysis and results can be found in Balman & Gamsızkan (2017).

Introduction

The classical nova V2491 Cyg is discovered by Nakano et al. (2008) in April 2008 (mag 7.7) on CCD frames in white light. The x-ray spectra that are obtained from different observatories ROSAT, *XMM-Newton Swift* revealed soft and hard x-ray components and complex absorption features during its outburst stage (Page et al. 2010; Ness et al. 2011; Pinto et al. 2012). We aim to reanalyse and model complex absorption features of the classical nova V2491 Cyg that are seen on the high resolution x-ray spectra obtained by *XMM-Newton* RGS 40 (2008 May 20.6) and 50 (2008 May 30.3) days after its outburst.

We divide the first observation into three spectra with respect to their count rates and identified them as regions. The three different count rate regions are labeled 1, 2, and 3 on the light curves (LC) as assumed in the spectral analysis and can be seen in Figure-1. Count rate of region1 is approximately 13 counts/s, region2 is ≈3 counts/s, region3 is ≈19 counts/s and the second observation is ≈2 counts/s. The spectral analysis and modelling is performed with SRON software SPEX version 2.05.04. The absorption component analysis is based on collisionally ionized hot absorber and a photoionized warm absorber models independent from the continuum model. The RGS data can be best fitted with two collisionally ionized hot absorber (HOT) and a photoionized warm absorber model (XABS) (plus a model for interstellar absorption (ISM) and dust absorption (AMOL)) together with a blackbody model (BB) and collisional ionization equilibrium model (CIE) for the continuum (`AMOL×HOT-ISM×(CIE+(HOT-1×HOT-2)×BB)`).

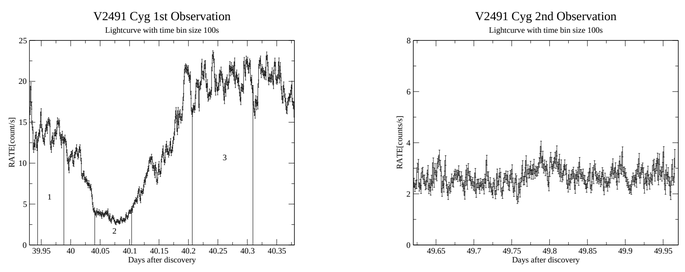

Figure 1: *XMM-Newton* RGS1 LC of V2491 Cyg. First observation is on the left and the second observation is on the right.

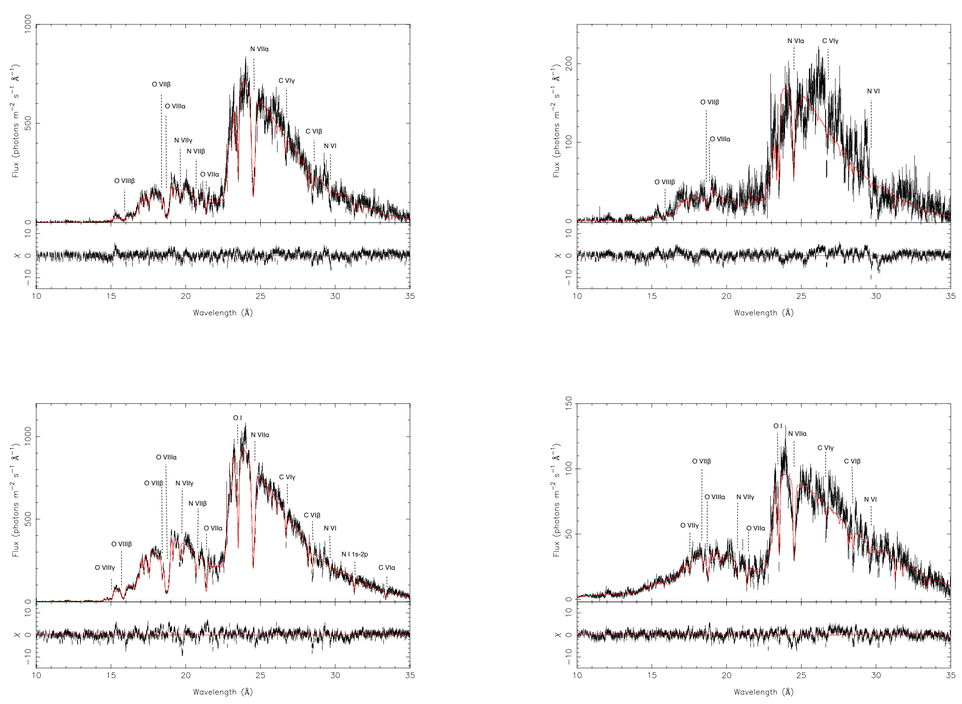

Figure 2: RGS 1+2 fluxed spectra extracted from the regions. The top left hand panel is region1, the top right hand panel is region2, the bottom left hand panel is region3 and the bottom right hand panel is the second observation.

Results

X-ray spectra shows deep and complex absorption features. We firstly derive two collisionally ionized hot absorber components from our fits. Figure-2 shows the X-ray spectrum with the two HOT absorber models and Table-1 gives the best fit spectral parameters. Our fits model the ionized absorption features simultaneously hence we could calculate a global velocity shift for the absorption component in the data originating from the nova wind and/or ejecta. Two different hot-absorber components have blueshifts in the range 2900-3800 km s^{-1} for the first and 2600-3600 km s^{-1} for the second observation that are consistent with ejecta or wind speeds. We find the equivalent hydrogen column density of the HOT (in equilibrium) absorbers in a range (0.6-18.0)$\times10^{23}$ cm^{-2} and (2.0-5.3)$\times10^{23}$ cm^{-2} on 40 and 50 days after outburst, respectively. The HOT components have temperatures $kT_1 \simeq 1.0-3.6$ keV and $kT_2 \simeq 0.4-0.87$ keV with rms velocities $\sigma_{v1} \sim 872$ km s^{-1} and $\sigma_{v2} \sim 56$ km s^{-1} that are consistent with shock temperatures in the X-ray wavelengths.

The continuum is modelled by collisional ionization equilibrium model (CIE) and blackbody model (BB). The BB temperatures are in the range 61-91 eV that yield a white dwarf (WD) mass of 1.15-1.3 M⊙. The Ne and Mg abundances are obtained from the fit of the CIE and and the interstellar absorption (cold Hot-ISM) model in the wavelength range 7-14.4 Å where the emission is prominent. A blackbody model of emission was also used as an additive model for the second-observation spectrum. The second BB component has an effective temperature 120-131 eV and effective radius about 10% of the WD. The model fit can be seen in Figure-3.

We derive C, N, O abundances of V2491 Cyg which shows a typical signature of H-burning with underabundant carbon C/C$_\odot$=0.3-0.5, and enhanced nitrogen N/N$_\odot$=5-7 and oxygen O/O$_\odot$=16-43. The high oxygen overabundance hints at a C-O WD. In addition to C,N,O we find abundances of the Si, S, Ar, Ca and Fe whose values can be seen in Table-1.

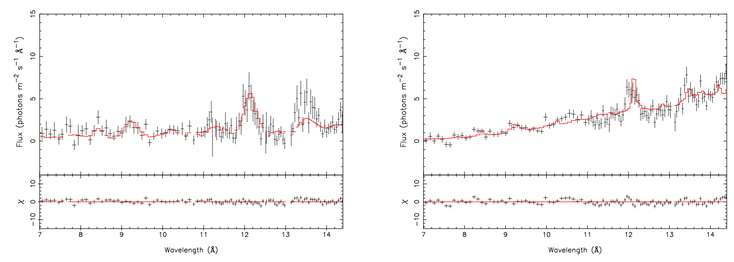

Figure 3: RGS1+2 fluxed spectrum of V2491 Cyg fitted in the range 7-14.4 Å. The left- and right-hand panels show the fit to the fluxed spectrum of region 3 and second-observation data, respectively.

The best fit χ^2_ν values with two hot absorbers can be seen in Table-1. The χ^2_ν values that we obtained show improvement with respect to the ones that achieved through the intrinsic photoionized absorber (warm absorber) fits in Pinto et al. (2012). We performed an F-test to check the significance of the improvement in the fits. F-test yields an improvement over 10σ in the three regions of the first observation whereas 1σ in the second observation.

We consider an additional third intrinsic absorber component originating in the shell/ejecta. We first apply third HOT component and calculated the significance of this component with respect to our previous work. F-test showed that the fits to the data of region 1, 2, and the second observation yield improvement of χ^2 values at a confidence level less than 30%. However, region3 spectrum resulted in a probability of 5×10^{-8} yielding an improvement over 5σ. Additionally, we tested the probability of having photoionized warm absorber component (XABS). We constructed a composite model (`AMOL×HOT-ISM×(CIE+(HOT-1×HOT-2×XABS)×(BB))`) which implies that there is some absorption from photoionized gas along with the main absorbers that are collisionally ionized. XABS model requires a grid of ionic column densities that can be calculated with the CLOUDY software assuming an ionizing continuum of blackbody radiation at 65 eV ($7.8\times10^5 K$). The resulting fits show that all the χ^2_ν values except the region2 fit (only by 3σ) are improved over 10σ significance with respect to the fits in Table-1. These improved fits are given in Table-2.

Table 1: The spectral parameters from the two-hot model best fit of the RGS spectrum of V2491 Cyg. Errors are calculated with 90% confidence level.

Model	Parameters	Region1	Region2	Region3	2^{nd} Obs.
BB	Norm	$1.53^{+0.39}_{-0.25}$	$0.23^{+0.86}_{-0.04}$	$0.40^{+0.47}_{-0.21}$	$0.02^{+0.05}_{-0.01}$
	kT (eV)	$68.5^{+0.9}_{-0.9}$	$64.5^{+0.6}_{-3.6}$	$88.4^{+2.7}_{-1.8}$	$75.7^{+9.1}_{-6.5}$
	L (10^{39} erg s^{-1})	2.18	0.23	1.92	0.05
CIE	Norm	$0.40^{+0.11}_{-0.09}$	$0.72^{+0.79}_{-0.32}$	$0.42^{+0.13}_{-0.05}$	$0.27^{+0.06}_{-0.1}$
	kT (keV)	$0.20^{+0.01}_{-0.01}$	$0.16^{+0.03}_{-0.02}$	$0.20^{+0.01}_{-0.01}$	$0.30^{+0.13}_{-0.03}$
	v_{mic} (km s^{-1})	2791	2791	2791^{+333}_{-288}	25068^{+1383}_{-951}
	Ne Abun.	2.45	2.45	$2.45^{+1.36}_{-0.92}$	$2.4^{+0.9}_{-0.9}$
	Mg Abun.	1.2	1.2	$1.2^{+1.0}_{-0.6}$	$1.98^{+0.70}_{-0.70}$
	L (10^{36} erg s^{-1})	1.31	1.78	1.38	0.77
HOT-1	N_H	$0.40^{+0.03}_{-0.03}$	$0.09^{+0.03}_{-0.01}$	$0.07^{+0.01}_{-0.01}$	$0.19^{+0.10}_{-0.02}$
	kT (keV)	$2.63^{+0.96}_{-0.56}$	$1.77^{+0.17}_{-0.12}$	$1.06^{+0.03}_{-0.03}$	$1.38^{+0.58}_{-0.12}$
	σ_v (km s^{-1})	872^{+25}_{-24}	827^{+61}_{-86}	879^{+12}_{-12}	114^{+18}_{-15}
	zv (km s^{-1})	-3186^{+51}_{-50}	-3699^{+113}_{-173}	-3128^{+30}_{-31}	-2636^{+47}_{-45}
HOT-2	N_H	$0.86^{+0.03}_{-0.03}$	$0.18^{+0.01}_{-0.02}$	$1.80^{+0.02}_{-0.02}$	$0.51^{+0.05}_{-0.05}$
	kT (keV)	$0.81^{+0.03}_{-0.03}$	$0.58^{+0.07}_{-0.11}$	$0.99^{+0.03}_{-0.03}$	$0.82^{+0.05}_{-0.45}$
	σ_v (km s^{-1})	54^{+8}_{-9}	< 9	56^{+4}_{-5}	60^{+7}_{-8}
	zv (km s^{-1})	-3180^{+71}_{-58}	-3038^{+6}_{-183}	-3194^{+30}_{-31}	-3550^{+36}_{-33}
Abun.	C	0.43	0.43	$0.43^{+0.07}_{-0.07}$	0.43
	N	5.2	5.9	$5.9^{+0.5}_{-0.9}$	5.9
	O	37.9	37.9	$37.9^{+5.8}_{-10.0}$	37.9
	Si	0.02	0.02	< 0.02	0.02
	S	0.02	0.02	$0.02^{+0.01}_{-0.01}$	0.02
	Ar	1.6	1.6	$1.6^{+3.9}_{-1.2}$	1.6
	Ca	0.01	0.01	< 0.01	0.01
	Fe	8.9	8.9	$8.9^{+3.8}_{-2.1}$	8.9
ISM	N_H	$3.89^{+0.06}_{-0.06}$	$3.84^{+0.06}_{-0.19}$	$3.26^{+0.05}_{-0.09}$	$2.4^{+0.3}_{-0.2}$
	kT (eV)	$1.11^{+0.03}_{-0.04}$	$1.20^{+0.02}_{-0.04}$	$1.01^{+0.02}_{-0.02}$	$0.8^{+0.3}_{-0.3}$
	N Abun.	1.16	1.16	$1.16^{+0.12}_{-0.12}$	1.16
	O Abun.	1.75	1.75	$1.75^{+0.04}_{-0.02}$	1.75
	Fe Abun.	0.95	0.95	$0.95^{+0.13}_{-0.12}$	0.95
AMOL	O_2	$0.34^{+0.13}_{-0.13}$	$2.3^{+0.2}_{-0.2}$	< 0.1	$1.3^{+0.1}_{-0.1}$
	$H_2O(ice)$	$5.5^{+0.3}_{-0.3}$	$7.8^{+0.5}_{-0.5}$	$4.77^{+0.13}_{-0.13}$	$7.2^{+0.2}_{-0.2}$
	CO	$1.28^{+0.13}_{-0.13}$	$0.27^{+0.2}_{-0.2}$	$0.1^{+0.07}_{-0.06}$	< 0.1
	χ^2_ν	1.80	2.4	2.86	2.3
	(d.o.f.)	(1415)	(1439)	(1440)	(1465)

Table 2: The spectral parameters from the two-hot model and one-xabs best fit of the RGS spectrum of V2491 Cyg. Errors are calculated with 90% confidence level.

Model	Parameters	Region1	Region2	Region3	2^{nd} Obs.
BB	Norm	$0.99^{+0.06}_{-0.06}$	$0.46^{+0.05}_{-0.05}$	$0.40^{+0.01}_{-0.01}$	$0.02^{+0.01}_{-0.01}$
	kT (eV)	$68.1^{+0.5}_{-0.5}$	$63.1^{+1}_{-0.8}$	$84.6^{+0.4}_{-0.4}$	$79.9^{+1.2}_{-1.2}$
	L (10^{39} erg s^{-1})	1.37	0.43	1.57	0.06
CIE	Norm	$0.97^{+0.47}_{-0.37}$	$1.14^{+0.71}_{-0.40}$	$0.42^{+0.13}_{-0.05}$	$0.55^{+0.04}_{-0.04}$
	kT (keV)	$0.18^{+0.02}_{-0.01}$	$0.17^{+0.02}_{-0.02}$	$0.19^{+0.01}_{-0.01}$	$0.26^{+0.01}_{-0.01}$
	$v_{\rm mic}$ (km s^{-1})	2914	2914	2914^{+612}_{-510}	22410^{+1688}_{-1466}
	Ne Abun.	2.45	2.45	$2.45^{+1.36}_{-0.92}$	$2.4^{+0.9}_{-0.9}$
	Mg Abun.	1.2	1.2	$1.2^{+1.0}_{-0.6}$	$1.98^{+0.70}_{-0.70}$
	L (10^{36} erg s^{-1})	1.34	1.49	1.18	0.88
HOT-1	N_H	$0.08^{+0.01}_{-0.01}$	$0.13^{+0.26}_{-0.05}$	$0.06^{+0.01}_{-0.01}$	$0.16^{+0.69}_{-0.02}$
	kT (keV)	$0.95^{+0.04}_{-0.04}$	$2.48^{+0.52}_{-0.35}$	$0.94^{+0.02}_{-0.02}$	$1.19^{+0.86}_{-0.20}$
	σ_v (km s^{-1})	892^{+43}_{-41}	634^{+131}_{-156}	932^{+23}_{-23}	133^{+31}_{-28}
	zv(km s^{-1})	-3304^{+83}_{-83}	-3805^{+229}_{-278}	-3250^{+51}_{-51}	-2826^{+88}_{-97}
HOT-2	N_H	$0.76^{+0.02}_{-0.02}$	$0.44^{+0.05}_{-0.24}$	$1.61^{+0.01}_{-0.01}$	$0.71^{+0.01}_{-0.14}$
	kT (keV)	$0.89^{+0.05}_{-0.04}$	$0.59^{+0.02}_{-0.1}$	$1.06^{+0.02}_{-0.02}$	$0.68^{+0.01}_{-0.19}$
	σ_v (km s^{-1})	< 37	< 20	35^{+14}_{-18}	< 17
	zv (km s^{-1})	-3309^{+84}_{-103}	-3073^{+161}_{-191}	-3334^{+38}_{-36}	-3660^{+75}_{-65}
XABS	N_H ($10^{20} cm^{-2}$)	$2.68^{+0.4}_{-0.3}$	$3.85^{+40}_{-2.56}$	$2.79^{+0.1}_{-0.1}$	$0.56^{+0.06}_{-0.06}$
	Log ξ	$2.04^{+0.14}_{-0.16}$	$3.64^{+1.35}_{-0.2}$	$2.18^{+0.05}_{-0.05}$	$0.41^{+0.08}_{-0.07}$
	σ_v (km s^{-1})	49^{+126}_{-18}	< 15831	53^{+10}_{-9}	195^{+78}_{-58}
	zv (km s^{-1})	-3013^{+100}_{-368}	-1093^{+1294}_{-343}	-2968^{+47}_{-44}	-3127^{+127}_{-118}
Abun.	C	0.38	0.38	$0.38^{+0.07}_{-0.07}$	0.38
	N	5.8	5.8	$5.8^{+0.2}_{-0.2}$	5.8
	O	15.9	15.9	$15.9^{+0.5}_{-0.5}$	15.9
	Si	0.06	0.06	< 0.06	0.06
	S	0.02	0.02	$0.02^{+0.02}_{-0.01}$	0.02
	Ar	0.5	0.5	< 0.5	0.5
	Ca	0.02	0.02	< 0.02	0.02
	Fe	8.9	8.9	$8.9^{+3.8}_{-2.1}$	8.9
ISM	N_H	$3.81^{+0.05}_{-0.05}$	$4.15^{+0.05}_{-0.06}$	$3.31^{+0.02}_{-0.02}$	$2.4^{+0.1}_{-0.1}$
	kT (eV)	$1.09^{+0.07}_{-0.3}$	$1.20^{+0.03}_{-0.05}$	$1.01^{+0.04}_{-0.04}$	$0.8^{+0.1}_{-0.1}$
	N Abun.	1.12	1.12	$1.12^{+0.13}_{-0.14}$	1.12
	O Abun.	1.68	1.68	$1.68^{+0.02}_{-0.02}$	1.68
	Fe Abun.	0.81	0.81	$0.81^{+0.13}_{-0.12}$	0.81
AMOL	O_2	$0.47^{+0.61}_{-0.03}$	$1.48^{+0.23}_{-0.24}$	< 0.4	$0.9^{+0.1}_{-0.1}$
	$H_2O(ice)$	$5.1^{+1.2}_{-0.1}$	$7.4^{+0.5}_{-0.5}$	$4.65^{+0.3}_{-0.7}$	$6.4^{+0.2}_{-0.2}$
	CO	$1.34^{+0.53}_{-0.03}$	$0.29^{+0.2}_{-0.2}$	$0.16^{+0.07}_{-0.06}$	< 0.2
	χ^2_ν	1.73	2.38	2.46	2.06
	(d.o.f.)	(1411)	(1435)	(1436)	(1463)

Notes. The BB norm and CIE norm in the tables are given in $10^{20} cm^2$ and $10^{58} cm^{-3}$ respectively. N_H for the HOT models are in $10^{24} cm^{-2}$ whereas N_H for he ISM-HOT model is in $10^{21} cm^{-2}$. zv indicates the velocity shift, σ_v is rms velocity. The XABS parameter Log ξ is given in erg cm s^{-1} and AMOL parameters are in 10^{17}cm^{-2}.

Conclusion

The analysis of the *XMM-Newton* RGS data yields two distinct hot collisionally ionized (in equilibrium) absorber components. The hot components with an addition of a warm photoionized component can be considered as the origin of the complex absorption features of the V2491 Cyg. Our work yields different temperatures, rms velocities, and equivalent column densities for the hot components originating in the shocked fast-moving ejecta and/or the wind. The difference can be as a result of high- and low-density regions with different turbulent conditions and temperatures in the ejecta and/or the wind indicating the inhomogeneity and mixed morphology of the outflow.

References

Balman, Ş., & Gamsızkan, Ç. 2017, A&A, 598, A129

Nakano, S., Beize, J., Jin, Z.-W., et al. 2008, IAU Circ., 8934, 1

Ness, J.-U. et al., 2011, ApJ, 733, 70

Page, K.L. et al., 2010, MNRAS, 401, 121

Pinto, C., Ness, J-U, Verbunt, F., Kaastra, J.S., Constantini, E., & Detmers, R.G., 2012, A&A, 543, A134

Acknowledgements

The authors acknowledge support from TÜBITAK, The Scientific and Technological Research Council of Turkey, through project 114F351.